mmWave Channel Stationarity Analysis of V2X Communications in an Urban Environment

Fidel Alejandro Rodríguez-Corbo [ID], Leyre Azpilicueta [ID], *Senior Member, IEEE*,
Mikel Celaya-Echarri [ID], *Member, IEEE*, Raed Shubair [ID], *Senior Member, IEEE*,
and Francisco Falcone [ID], *Senior Member, IEEE*

Abstract—**Vehicular communication channels are subject to high nonstationarity mainly characterized by the scatterers' and/or transceivers' high mobility. In this sense, this letter presents a characterization of the channel quasi-stationarity regions (QSR) in a V2X generic high-dense urban environment at millimeter wave frequencies (28 GHz). Results are extracted from multiple snapshot simulations by means of a three-dimensional ray-launching algorithm inducing the continuous mobility of the vehicles on the scene and validated with an experimental campaign of measurements in the real scenario. The average power delay profile correlation matrix is used as a descriptor of the channel nonstationarity and the mean correlation is outlined for several thresholds. The obtained QSR results are consistent with the related works reported in the literature. Finally, the effects of these QSR in small- and large-scale parameters are assessed as per threshold considerations.**

Index Terms—**Correlation matrix, nonstationarity, quasi-stationarity regions (QSRs), three-dimensional ray-launching (3-D-RL), V2X.**

I. INTRODUCTION

VEHICULAR communications have received an increased attention in recent years [1], [2]. These systems differ from conventional ones in several aspects [3], where the most distinctive are the high mobility of the medium and the relatively low antennas heights, in which vehicle-to-vehicle (V2V) link cases play an important role in line-of-sight (LoS) conditions. Directly

Fidel Alejandro Rodríguez-Corbo is with the School of Engineering and Sciences, Tecnologico de Monterrey, Monterrey 64849, Mexico (e-mail: a00829477@tec.mx).

Leyre Azpilicueta is with the Department of Electric, Electronic and Communication Engineering and the Institute of Smart Cities, Public University of Navarre (UPNA), 31006 Pamplona, Spain (e-mail: leyre.azpilicueta@unavarra.es).

Mikel Celaya-Echarri is with the Department of Statistics, Computer Science and Mathematics, Public University of Navarre (UPNA), 31006 Pamplona, Spain (e-mail: mikelcelaya@tec.mx).

Raed Shubair is with the Department of Electrical and Computer Engineering, New York University Abu Dhabi, Abu Dhabi 129188, UAE (e-mail: raed.shubair@nyu.edu).

Francisco Falcone is with the Department of Electric, Electronic and Communication Engineering and the Institute of Smart Cities, Public University of Navarre (UPNA), 31006 Pamplona, Spain, and also with the School of Engineering and Sciences, Tecnologico de Monterrey, Monterrey 64849, Mexico (e-mail: francisco.falcone@unavarra.es).

Digital Object Identifier 10.1109/LAWP.2023.3243696

related to the high mobility of the medium is the nonstationary channel behavior, which is mainly affected by the transceivers' and/or scatterers' mobility. The use of channel models based on the wide sense stationary and uncorrelated scattering (WSSUS) assumption have been widely used in traditional models. Nevertheless, abundant theoretical and experimental studies have shown that WSSUS properties are only valid in short periods of time [4], and thus not valid to describe the radio channel in vehicular environments. As a result, some vehicular channel models have included the nonstationarity of the environment in their implementations, considering different approaches.

The main approaches to assess the degree of nonstationarity come in the form of some measure of correlation or spectral divergences (SDs) that can be used to develop statistic/stochastic channel models. In this sense, the correlation matrix distance (CMD) is widely used in multiple-input–multiple-output (MIMO) systems to characterize the similarity between two correlation matrixes [5]. In [6], a V2V measurement campaign at 5.3 GHz is described using the CMD to evaluate the channel nonstationarity. In [7], a combination of CMD, SD, and shadow fading correlation, are used to characterize the nonstationary communication channel for different V2V scenarios at 5.3 GHz. Another algorithm based on the local scattering function (LSF) is used in [8], evaluating its collinearity to quantify, in this case, the time interval over which the channel can be approximated as WSSUS for a V2V scenario at 5 GHz. Another LSF approach is implemented in [9] at 2.53 GHz, in which the mean stationarity time is found for the presented measurement setup. Li et al. [10] introduced various V2V scenarios at 5.9 GHz, where the nonstationarity is analyzed based on a correlation method using the power delay profile (PDP). This approach was also implemented in [11] for complex scenarios like viaducts, tunnels, and cuttings. Finally, in [12], the correlation distance in a millimeter wave (mmWave) study of an outdoor microcellular scenario is presented, with an average correlation distance of 0.9 m, suggesting being shorter than those referenced in sub-6 GHz. Overall, the nonstationary characteristics of the vehicular communication channels on the mmWave spectrum have been disproportionally less addressed in the literature. The high transfer speed and low latency at these frequency bands make them a possible path to more accurate and effective vehicular communications. Thus, further studies are needed for millimeter band frequency systems use cases.

The aim of this letter is encouraged by the need to provide and validate an accurate nonstationarity simulation approach to estimate and characterize the quasi-stationarity regions (QSRs) in vehicular environments at mmWave frequency bands, regardless site-specific conditions. With the aim to fill this gap,

in this letter, the vehicular channel nonstationarity of a V2I generic link operating at 28 GHz frequency in a high-dense urban scenario is analyzed, by means of an in-house deterministic three-dimensional ray launching (3-D-RL) algorithm, extendable without loss of generality to the V2X case. Using the correlation matrix for all the receiver's displacement, an in-deepness channel nonstationarity analysis is presented with its corresponding quasi-stationarity distances, considering the most typically used thresholds. A complete self and cross comparison with a campaign of measurements in the real scenario and the related works in the literature, respectively, is provided for validation and verification purposes. Finally, QSR results are discussed, and conclusions are stated.

II. Channel Nonstationarity Modeling Technique

An in-house developed 3-D-RL simulation tool [13] has been used in order to analyze the vehicular nonstationarity channel properties. The 3-D-RL algorithm is based on geometrical optics and the uniform theory of diffraction, where the spherical coordinate system is used to launch rays at an elevation angle θ and an azimuth angle $\emptyset$ in the complete volume of the considered scenario. General simulation code parameters, such as frequency of operation (28 GHz), number of multipath reflections (4 rebounds), separation angle between rays (θ, $\emptyset$) of (0.5°, 1°), cuboids dimensions (0.4/0.1 m), and transmitted power (24 dBm), are introduced as input parameters in the algorithm. It must be remarked that a full detailed 3-D scenario is created for simulation, modeling all the elements of the real environment, from relevant scatterers, such as buildings, vehicles, vegetation, and pedestrians, to single elements as traffic lights, trees, or benches, including the transmitters and receivers with all their corresponding features. Moreover, their material properties are considered, given the relative permittivity and conductivity at the frequency range of operation of the system under analysis [14]. Finally, the frequency dispersive effects due to the vehicles' movement can be analyzed as well, considering different velocities of the vehicles. The channel nonstationarity analysis is performed using continuous and exhaustive deterministic simulations of different temporal snapshots of the dynamic scenario. Thus, in order to determine the stationarity regions, the average power delay profiles (APDPs) are extracted as follows to eliminate small-scale effects:

$$\overline{P_h}\,(x_i, \tau) = \frac{1}{N} \sum_{i}^{i+N-1} |h(i, \tau)|^2 \qquad (1)$$

where $\overline{P_h}(x, \tau)$ is the APDP at the indexed position at τ delay, N is the length of sliding window, i is the indexed position of the vehicle along the route, and $h(i, \tau)$ is the channel response at the indexed position. A spatial area of 40λ [7] has been considered for this average, which corresponds to approximately 0.4 m operating at 28 GHz. The 3-D-RL simulator step in the direction of movement has been set to approximately 10λ (0.1 m) and a sliding window of four steps (approx. 40λ) has been used to average the PDPs. Thus, the multipath components can be captured in each spatial section and the overall APDP is obtained for that specific displacement unit. Then, using (2) and the data generated, the correlation coefficient $\rho(x_i, x_j)$ between the APDPs is determined for the variations of Δr (defined as one sliding step of 0.1 m)

$$\rho(x_i, x_j) = \frac{\sum_0^{all\ \tau}\left(\overline{P_h}(x_i, \tau) * \overline{P_h}(x_j, \tau)\right)}{\max\left\{\sum_0^{all\ \tau}\left(\overline{P_h}(x_i, \tau)^2\right), \sum_0^{all\ \tau}\left(\overline{P_h}(x_j, \tau)^2\right)\right\}} \qquad (2)$$
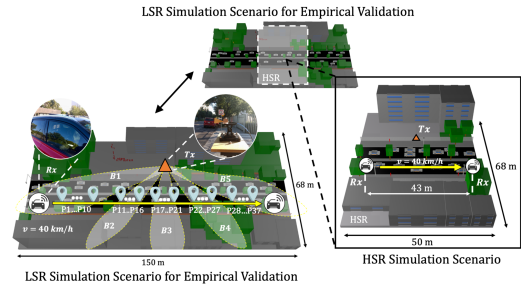

Fig. 1. Schematic views of the vehicular urban scenario modeled for both simulations: LSR (measurement campaign scheme for empirical validation) and HSR (QSRs' calculations setup), considering the vehicle's trajectories analyzed and the corresponding transceivers' locations for each resolution.

where $\rho(x_i, x_j)$ is the correlation coefficient, and i and j are the position index of the receiver (Rx), using Δr as the unit of displacement. Finally, if the level of permissiveness between the maximum correlation and a predefined threshold is determined, the channel is considered quasi-stationary within these sections, meeting the restrictions of this assumption.

III. Scenario Description

The selected scenario is a typical vehicular urban environment, composed by a two-way avenue section of 150 m long with abundant traffic and an intermediate checkpoint with medium-height vegetation, where a V2I communication link has been considered, characterized by a 2 m height road-side unit (RSU) located center stage. This specific setup is subject to a higher state of NLoS conditions due to the low height of the transmitter (Tx) as well as the high surrounding vehicular mobility and the presence of multiple scatterers, which represent an influencing factor in the communication link characteristics. In Fig. 1, a schematic view of the vehicular urban scenario model is depicted, considering the vehicle's trajectories analyzed and the corresponding transceivers' locations. The selected scenario has been simulated with two different spatial resolutions: a low spatial resolution (LSR) for the empirical comparison and validation in the full scenario (150 m length) and a high spatial resolution (HSR) for the QSRs' calculations, in a partial section of the total scenario (50 m length). A resolution of 40λ (approx. 0.4 m) has been implemented in the full volume scenario, defined as LSR simulation scenario for empirical validation, whereas a more restrictive 10λ (approx. 0.1 m) resolution has been applied in the 50 m length scenario, defined as HSR simulation scenario. This approach has been followed due to the high computational cost needed to obtain the raw data for the calculation of the QSRs.

During the measurement campaign, the RSU was emulated using a 16° directional half-power beam antenna for the Tx, with five fixed angular beam positions (B1–B5) with a 21° sweep between beams. For the Rx, a portable FieldFox spectrum analyzer has been selected, using an omnidirectional antenna with 3 dBi gain located fixed in the roof window of a conventional SUV vehicle, associated with a low-noise amplifier with an extra 27 dBi gain (see the LSR simulation scenario for empirical validation's schematic view of Fig. 1 for further reference). In order to reproduce the real dynamic conditions of the measurements campaign, a high vehicular density was considered for simulations, with 30 and 18 vehicles per the LSR and the HRS snapshot, respectively, all at a constant speed of 40 km/h, which is the allowed and expected real speed in
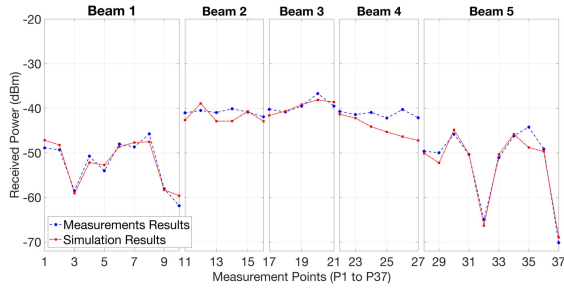
Fig. 2.   Experimental measurements and 3-D-RL simulation comparison along the different beams B1, …,B5 depicted in Fig. 1.
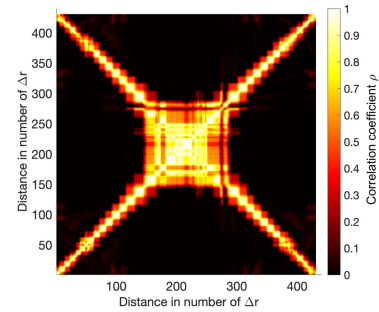

Fig. 3.   Correlation matrix for the moving receiving vehicle.

Fig. 4.   Mean correlation versus the different distance variation snapshots.

this avenue. Both simulations were performed with full omnidirectional Tx and Rx antennas in order to retain all scatterers interactions information and the required LSR directional beam pattern (B1–B5) was synthetize in a postprocess for the empirical comparison. In Fig. 2, the received power comparison between the LSR simulation and the measurement campaign results is presented.

Discrete location results (P1–P37) have been extracted from the empirical measurements to allow simulation comparison and verification. Considering the Rx's trajectory and the Tx fixed location, different areas were covered by the performed beams, based on the Tx's radiation pattern. Therefore, each specific road area has been divided in different sections with equidistant spacing, considering the spatial road path differences in each beam coverage area. Thus, 10 sections have been defined for beam B1 (P1–P10) and B5 (P28–P37), 6 sections for beam B2 (P11–P16) and B4 (P22–P27), and 5 sections for beam B3 (P17–P21), which are represented in the LSR scenario for empirical validation of Fig. 1 and correspond with the same locations used for comparison in Fig. 2. The comparison shows good agreement between them, with a mean error not exceeding 4 dB in each section and a total mean error of 1.9 dB. It must be pointed out that these simulation uncertainties can be explained by the inherent modeling difficulties to represent the exact reality picture of the scenario under evaluation, in terms of scatterers' location, or possible vegetation blockage, as well as the vehicles' locations and their true relative speed.

IV. SIMULATION RESULTS

Once the parameters of the 3-D-RL simulator have been established and validated in the measurement campaign under similar vehicle density conditions, using the HSR simulation, the main scenario's scatterers principle characteristics can be captured and analyzed in deepness. In this sense, to evaluate the nonstationarity of a vehicular receiver, an antenna located on top (1.5 m height) of one of the vehicles on the avenue is taken as a reference, and simulations were performed along its total travel distance across the scenario. Although the total dimension of the analyzed HSR simulation scenario and the total travel distance of the receiving vehicle is 50 m, the specific location of the antenna in the middle of the vehicle's roof corresponds with an effective 43 m travel distance (from 3 to 46 m approx.). See the HSR simulation scenario's schematic view of Fig. 1 for further reference.

A. Correlation Matrix

The correlation matrix is used to compute the correlation coefficients for the entire trajectory of the vehicle along the road, as a function of the distance parameter Δr following (2). As the total effective travel distance of the receiving vehicle is 43 m, the
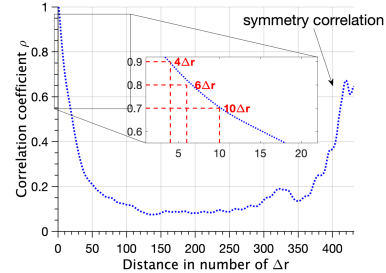
arrangement of the Δr is between 1 and $430\Delta r$ for the correlation function, which corresponds with 430 snapshots implemented in the 3-D-RL simulation. In Fig. 3, the correlation matrix for the receiving vehicle along the trajectory is presented. A wide area of stationarity is depicted from approximately 150 to $270\Delta r$, which corresponds with the vehicle's partial trajectory between the meters 15 and 27, which in turn places the Rx approximately in the center of the stage and in the shortest possible distance from the Tx. In this specific V2I setup, LoS and/or ground reflections components prevail in most APDPs when considering the Rx crossing in front of the Tx. The second-order components with the highest intensity are predominantly reflection components from the scatterers behind the vehicle, caused by the surrounding large buildings. Thus, the direct influence of the LoS components as well as the remanence of reflective components in nearby buildings along the corresponding APDPs in this analyzed area keep the channel relatively stationary for longer periods.

B. Mean Correlation and Threshold

Fig. 4 presents the mean correlation versus the distance displacement Δr with respect to each simulated snapshot locations from the correlation matrix.

The mean correlation is shown for the complete vehicle's trajectory (43 m), from a total correlation at the starting point $\Delta r = 1$ to the final location $430\Delta r$ on the way. Although the symmetry correlation influences across many distances the mean correlation, this behavior is more evident from $350\Delta r$, as there is a constant decreasing number of trajectories with large displacements. Overall, to consider a quasi-stationarity distance, a threshold must be determined from which all the paths contained between this threshold and the maximum correlation are considered quasi-stationary. The determination of a precise threshold is a criterion for debate, and many considerations specific to the application for which this area of quasi-stationarity is intended to be used, come to the fore. In Fig. 4, three of the most typically used thresholds in the stationarity characterization regions [10], [11], and their corresponding distances to their associated

TABLE I
CROSS-COMPARISON OF QUASI-STATIONARITY REGIONS FOR DIFFERENT SCENARIOS, METHODS, AND FREQUENCIES

Ref.	Scenario	Comm.	Method	Freq. (GHz)	Vel. (km/h)	Threshold	QSR (m)
[15]	Suburban	V2I	LSF/CCF	1.35	40	0.95/–	6.3
[16]	Tunnel	V2I	CCF	1.35	90	–	8.25
[17]	Highway opposite direction	V2V	LSF	2.53	93.6	0.9	9.36
[18]	Highway same direction/ Urban	V2V	PDPC	5.22	80/50	0.8	18.25/9.51
[8]	Highway same direction/ Urban	V2V	LSF	5.2	90/30	0.9	36.97/11.76
[7]	Suburban LOS	V2V	CMD	5.3	30–40	0.8	10.18
[6]	Campus/ Highway/Suburban/Urban	V2V	CMD	5.3	7.5	0.8	10–40
[19]	Crossroad	V2V	CMD	5.3	10	0.8	4.52(LOS)/2.71(NLOS)
[10]	Dense urban / Urban crossroad	V2V	PDPC	5.9	18/37.08	0.8	9.7/10.17
[11]	Viaduct/Tunnel/Cutting	V2V	PDPC	5.9	10–50	0.8	10.2/13.5/7.54
[12]	Urban	V2I	PDPC	27.85	0.54	0.9	0.9
[20]	Highway	V2I	RUN test	28	100	–	0.06–0.25
[21]	Urban	V2I	CP (RT)	28	–	0.7	0.43
This work	Urban	V2I	PDPC (RT)	28	40	0.7/0.8/0.9	1/0.6/0.4

*LSF: local scattering function; CCF: channel correlation function; CMD: correlation matrix distance; PDPC: power delay profile correlation; CP: correlation power; RT: ray tracing.
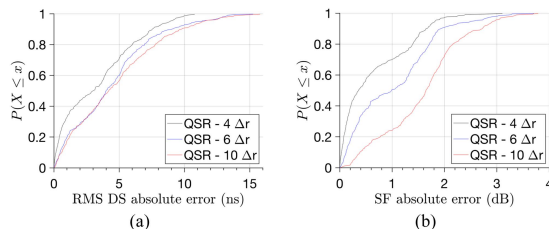

Fig. 5. (a) RMS DS absolute error, and (b) SF absolute error, for each QSR.

regions, are framed. The selected thresholds are 0.7, 0.8, and 0.9, which correspond to QSR of $10\Delta r$, $6\Delta r$, and $4\Delta r$, respectively. Considering that the deterministic step Δr used in this letter is 0.1 m, the QSR corresponds to 1, 0.6, and 0.4 m, respectively.

These areas capture the channel characteristics during which the signal propagation changes differ in correspondence to the selected threshold. Thus, the classification of these areas with the identification and characterization of small- and large-scale parameters and their corresponding influence, leads to a potential reduction in the required number of deterministic simulations, considering the consequent error. Finally, a full comparison of the obtained QSR results with related works in the literature is presented in Table I, showing good agreement.

C. RMS Delay Spread and Shadow Fading

As stated, QSR can reduce considerably the number of deterministic simulations needed to capture the underlying characteristics of the propagation phenomena. It also means that the sliding window for the APDP can be extended to cover the respective QSR, as the main characteristics of the channel are assumed quasi-stationary and only adding a relative error as per each threshold consideration. A second-order statistic like the root mean square delay spread (rms DS) is considered a good measure of the dispersiveness of the multipath channel and is closely related to the coherence bandwidth. The absolute error deviation of this small-scale parameter with respect to an increase in the APDP window can be a good criterion as how well the QSR capture the undelaying parameter. Fig. 5(a) shows the empirical cumulative distribution function (CDF) of the rms DS absolute error for each QSR. The mean absolute errors (MAEs) are 3.32, 4.39, and 4.71 ns for each QSR (4, 6, and $10\Delta r$), respectively. As expected, the MAE is lower as the window/QSR decreases, which is also related to higher correlation coefficient between underlying PDPs. Although large-scale parameters are slowly changing, assuming a QSR can also impact on its characterization. The shadow fading (SF) is one of these relevant

TABLE II
SMALL- AND LARGE-SCALE PARAMETERS SUMMARY ERROR

	RMS DS		SF	
	MAE	σ	MAE	σ
QSR - $4\Delta r$	3.32 ns	2.88 ns	0.65 dB	0.66 dB
QSR - $6\Delta r$	4.39 ns	3.30 ns	1.02 dB	0.80 dB
QSR - $10\Delta r$	4.71 ns	3.54 ns	1.58 dB	0.81 dB

parameters. For this analysis, a close in free space path loss model (CI model) [22] is fitted to the received power, and the SF is assumed to be the difference between the CI model and the path loss at the Rx position. Fig. 5(b) shows the empirical CDF of the SF absolute error for each QSR. Following the previous trend, the MAE decreases with the reduction in QSR, although the maximum difference in MAE is less than 1 dB. A summary of this small- and large-scale parameters are presented in Table II.

For typical values of SF, both the MAE and the standard deviation are not strongly affected by the increase in QSR. As expected for a large-scale parameter, this change has little impact in its characteristics. However, the rms DS standard deviation show more dispersiveness, considering that typical rms DS at these frequency bands are in the order of few tens of nanoseconds.

V. CONCLUSION

QSR can define time-changing statistics that are typically assumed to be constant in WSSUS channels, thus the characterization of this regions is of relevance to nonstationarity channels. This letter describes the QSR for different thresholds and evaluates their effects on small- and large-scale parameters like the rms DS and SF. A cross-comparison with similar works in the literature has been presented, showing good agreement. The considered scenario, the followed approach, frequency, and velocity play a key role in the QSR analysis. Results show that for mean correlation thresholds of 0.9, 0.8, and 0.7, the QSR span from 0.4, 0.6, and 1 m, respectively, showing a decrease in the QSR at mmWave compared with sub-6 GHz schemes. The MAE and standard deviation of the residual absolute error, introduced assuming larger QSR, increases in both cases (rms DS and SF), although a lower restriction in the threshold selection may not affect considerably the SF, as expected on a large-scale parameter. This increment in the rms DS absolute error dispersiveness for each QSR can ultimately influence important parameters like the coherence bandwidth. In general, the use of QSR leads to a potential reduction in the required deterministic simulations, considering the consequent error bounded to the mean correlation coefficient.

REFERENCES

[1] P. K. Singh, S. K. Nandi, and S. Nandi, "A tutorial survey on vehicular communication state of the art, and future research directions," *Veh. Commun.*, vol. 18, Aug. 2019, Art. no. 100164.

[2] L. Azpilicueta, C. Vargas-Rosales, F. Falcone, and A. V. Alejos, *Radio Wave propagation in Vehicular Environments*. London, U.K.: Institution of Engineering and Technology, 2020.

[3] F. A. Rodriguez-Corbo, L. Azpilicueta, M. Celaya-Echarri, A. V. Alejos, and F. Falcone, "Propagation models in vehicular communications," *IEEE Access*, vol. 9, pp. 15902–15913, 2021.

[4] L. Liang, H. Peng, G. Y. Li, and X. Shen, "Vehicular communications: A physical layer perspective," *IEEE Trans. Veh. Technol.*, vol. 66, no. 12, pp. 10647–10659, Dec. 2017.

[5] M. Herdin, N. Czink, H. Ozcelik, and E. Bonek, "Correlation matrix distance, a meaningful measure for evaluation of non-stationary MIMO channels," in *Proc. IEEE 61st Veh. Technol. Conf.*, 2005, pp. 136–140.

[6] O. Renaudin, V.-M. Kolmonen, P. Vainikainen, and C. Oestges, "Non-stationary narrowband MIMO inter-vehicle channel characterization in the 5-GHz band," *IEEE Trans. Veh. Technol.*, vol. 59, no. 4, pp. 2007–2015, May 2010.

[7] R. He et al., "Characterization of quasi-stationarity regions for vehicle-to-vehicle radio channels," *IEEE Trans. Antennas Propag.*, vol. 63, no. 5, pp. 2237–2251, May 2015.

[8] A. Paier et al., "Non-WSSUS vehicular channel characterization in highway and urban scenarios at 5.2 GHz using the local scattering function," in *Proc. Int. ITG Workshop Smart Antennas*, 2008, pp. 9–15.

[9] M. Herdin, N. Czink, H. Ozcelik, and E. Bonek, "Correlation matrix distance, a meaningful measure for evaluation of non-stationary MIMO channels," in *Proc. IEEE 61st Veh. Technol. Conf.*, 2005, pp. 136–140.

[10] F. Li, W. Chen, and Y. Shui, "Analysis of non-stationarity for 5.9 GHz channel in multiple vehicle-to-vehicle scenarios," *Sensors*, vol. 21, no. 11, May 2021, Art. no. 3626.

[11] M. Yang et al., "Non-stationary vehicular channel characterization in complicated scenarios," *IEEE Trans. Veh. Technol.*, vol. 70, no. 9, pp. 8387–8400, Sep. 2021.

[12] R. Wang et al., "Stationarity region of mm-wave channel based on outdoor microcellular measurements at 28 GHz," in *Proc. IEEE Mil. Commun. Conf.*, 2017, pp. 782–787.

[13] L. Azpilicueta, C. Vargas-Rosales, and F. Falcone, "Intelligent vehicle communication: Deterministic propagation prediction in transportation systems," *IEEE Veh. Technol. Mag.*, vol. 11, no. 3, pp. 29–37, Sep. 2016.

[14] L. Azpilicueta et al., "Fifth-generation (5G) mm-wave spatial channel characterization for urban environments' system analysis," *Sensors*, vol. 20, no. 18, Sep. 2020, Art. no. 5360.

[15] M. Yusuf et al., "Stationarity analysis of V2I radio channel in a suburban environment," *IEEE Trans. Veh. Technol.*, vol. 68, no. 12, pp. 11532–11542, Dec. 2019.

[16] M. Yusuf et al., "Experimental study on the impact of antenna characteristics on non-stationary V2I channel parameters in tunnels," *IEEE Trans. Veh. Technol.*, vol. 69, no. 11, pp. 12396–12407, Nov. 2020.

[17] D. Czaniera et al., "Investigation on stationarity of V2V channels in a highway scenario," in *Proc. 13th Eur. Conf. Antennas Propag.*, 2019, pp. 1–5.

[18] Q. Wang, D. W. Matolak, and B. Ai, "Shadowing characterization for 5-GHz vehicle-to-vehicle channels," *IEEE Trans. Veh. Technol.*, vol. 67, no. 3, pp. 1855–1866, Mar. 2018.

[19] R. He et al., "Vehicle-to-vehicle radio channel characterization in crossroad scenarios," *IEEE Trans. Veh. Technol.*, vol. 65, no. 8, pp. 5850–5861, Aug. 2016.

[20] J.-J. Park, J. Lee, K.-W. Kim, M.-D. Kim, H.-K. Kwon, and K. C. Lee, "Wide-sense stationarity of millimeter wave expressway channels based on 28 GHz measurements," in *Proc. IEEE 90th Veh. Technol. Conf.*, 2019, pp. 1–5.

[21] Z. Cui, Z. Zhong, K. Guan, and D. He, "An acceleration method for ray-tracing simulation based on channel quasi-stationarity regions," in *Proc. 12th Eur. Conf. Antennas Propag.*, 2018, pp. 1–5, doi: 10.1049/cp.2018.1198.

[22] T. S. Rappaport, G. R. MacCartney, M. K. Samimi, and S. Sun, "Wideband millimeter-wave propagation measurements and channel models for future wireless communication system design," *IEEE Trans. Commun.*, vol. 63, no. 9, pp. 3029–3056, Sep. 2015.